Acta Pharmaceutica Sinica B 2025;15(2):876–891

Chinese Pharmaceutical Association
Institute of Materia Medica, Chinese Academy of Medical Sciences

Acta Pharmaceutica Sinica B

www.elsevier.com/locate/apsb
www.sciencedirect.com

ORIGINAL ARTICLE

Celastrol directly targets LRP1 to inhibit fibroblast-macrophage crosstalk and ameliorates psoriasis progression

Yuyu Zhu[a,b,*,†], Lixin Zhao[b,†], Wei Yan[c,†], Hongyue Ma[a,†], Wanjun Zhao[b], Jiao Qu[b,d], Wei Zheng[b], Chenyang Zhang[b], Haojie Du[b], Meng Yu[a], Ning Wan[e], Hui Ye[e], Yicheng Xie[f], Bowen Ke[g], Qiang Xu[b], Haiyan Sun[h,*], Yang Sun[b,d,*], Zijun Ouyang[h,*]

[a]*Jiangsu Collaborative Innovation Center of Chinese Medicinal Resources Industrialization, and Jiangsu Key Laboratory for High Technology Research of TCM Formulae, College of Pharmacy, Nanjing University of Chinese Medicine, Nanjing 210023, China*
[b]*State Key Laboratory of Pharmaceutical Biotechnology and Department of Rheumatology and Immunology, Nanjing Drum Tower Hospital, the Affiliated Hospital of Nanjing University Medical School, School of Life Sciences, Nanjing University, Nanjing 210008, China*
[c]*Department of Dermatology and Venereology, West China Hospital, Sichuan University, Chengdu 610041, China*
[d]*Jiangsu Key Laboratory of New Drug Research and Clinical Pharmacy, Xuzhou Medical University, Xuzhou 221004, China*
[e]*Jiangsu Provincial Key Laboratory of Drug Metabolism and Pharmacokinetics, State Key Laboratory of Natural Medicines, China Pharmaceutical University, Nanjing 210009, China*
[f]*The Children's Hospital, Zhejiang University School of Medicine, National Clinical Research Center for Child Health, Hangzhou 310052, China*
[g]*Department of Anesthesiology, West China Hospital and State Key Laboratory of Biotherapy, Sichuan University, Chengdu 610041, China*
[h]*School of Food and Drug, Shenzhen Polytechnic University, Shenzhen 518055, China*

Received 29 July 2024; received in revised form 12 November 2024; accepted 22 November 2024

*Corresponding authors.
E-mail addresses: yangsun@nju.edu.cn (Yang Sun), ouyangzijun@szpu.edu.cn (Zijun Ouyang), susan@szpu.edu.cn (Haiyan Sun), yuyuzhu@njucm.edu.cn (Yuyu Zhu).
[†]These authors made equal contributions to this work.
Peer review under the responsibility of Chinese Pharmaceutical Association and Institute of Materia Medica, Chinese Academy of Medical Sciences.

https://doi.org/10.1016/j.apsb.2024.12.041

KEY WORDS

Psoriasis;
Fibroblast;
CCL2;
Celastrol;
LRP1;
Macrophage;
c-Jun;
Drug target

Abstract Psoriasis is an incurable chronic inflammatory disease that requires new interventions. Here, we found that fibroblasts exacerbate psoriasis progression by promoting macrophage recruitment *via* CCL2 secretion by single-cell multi-omics analysis. The natural small molecule celastrol was screened to interfere with the secretion of CCL2 by fibroblasts and improve the psoriasis-like symptoms in both murine and cynomolgus monkey models. Mechanistically, celastrol directly bound to the low-density lipoprotein receptor-related protein 1 (LRP1) β-chain and abolished its binding to the transcription factor c-Jun in the nucleus, which in turn inhibited CCL2 production by skin fibroblasts, blocked fibroblast−macrophage crosstalk, and ameliorated psoriasis progression. Notably, fibroblast-specific LRP1 knockout mice exhibited a significant reduction in psoriasis like inflammation. Taken together, from clinical samples and combined with various mouse models, we revealed the pathogenesis of psoriasis from the perspective of fibroblast-macrophage crosstalk, and provided a foundation for LRP1 as a novel potential target for psoriasis treatment.

1. Introduction

Psoriasis is a persistent autoimmune disease caused by genetic, immune, and infectious factors characterized by excessive epidermal proliferation and a chronic inflammatory reaction in the dermis. Erythema and scaling are the main clinical manifestations, which are prone to recurrence and even last for life[1,2]. Psoriasis affects 125 million people worldwide, with a prevalence of 2%−3% in Europe and the United States[3], and it is on a certain upward trend. Existing treatments are efficient and have tremendously changed psoriasis care[4].

In recent years, extensive research has concluded that psoriasis primarily arises from the disruption of the skin's inflammatory microenvironment, leading to massive inflammatory cell infiltration and overexpression of inflammatory factors. The IL-23/Th17 cell axis plays a critical component in the pathogenesis of psoriasis. Dendritic cells and macrophages secrete IL-23 in the dermis of psoriasis, activating Th17 cells[5,6]. Activated Th17 cells then release a range of inflammatory cytokines, such as IL-22, TNFα, IL17A, IL17F, and IL-6. Among them, IL17 A/F and IL-22 act on keratinocytes, causing typical pathological changes of psoriasis such as hyperkeratosis, abnormal epidermal proliferation, and hypertrophy of the spinous layer. This inflammatory milieu prompts keratinocytes to produce additional IL-23 and other inflammatory mediators and chemokines, establishing a positive feedback loop[7−9] that perpetuates and intensifies the chronic inflammatory state in psoriasis. However, the number of fibroblasts in the skin is not negligible and their role in psoriasis has rarely been studied.

The dermis and subcutaneous tissues of the skin contain a large number of fibroblasts, which were previously thought to synthesize and secrete extracellular matrix components such as collagen to perform structural functions[10,11]. In recent years, however, it has been found that the non-structural functions of fibroblasts should not be ignored[12,13]. Chen's group[14] found that fibroblasts are essential for the development of vitiligo, a skin autoimmune disease and that an interplay system formed by fibroblasts and $CD8^+$ T cells plays a key role in vitiligo. Fibroblasts are key cells in the production of early chemokines, and their activation is induced by tissue injury, microbial infection, or changes in the local microenvironment, producing a variety of chemokines that initiate the inflammatory response and act on themselves and other cells in an autocrine or paracrine manner. The release of high levels of cytokines by fibroblasts through paracrine secretion may be an important factor in the over-proliferation of keratinocytes[15,16]. Fibroblasts may also promote IL-23 secretion by dendritic cells and exacerbate psoriasis progression through the IL-23/Th17 cell axis. Fibroblasts can also influence the function of adherent cells by expressing adhesion factors, receptors or surface markers to adhere to, for example, lymphocytes and mast cells[17]. We hypothesize that the dermal abundance of fibroblasts acts as an "adjuvant-like" signal amplifier in the body's sensing of self- or exogenous antigens and the recruitment of immune cells, which contributes to the chronicity of psoriasis.

In our study, we analyze single-cell multi-omics data from psoriatic patients and healthy individuals, finding increased fibroblast−macrophage communication in psoriasis lesions, which contributes to disease progression. We screened a natural product library for compounds that interfere with fibroblast−macrophage communication, identifying celastrol. Celastrol directly targets LRP1, inhibiting fibroblast secretion of CCL2 and thereby preventing psoriasis-like progression by reducing CCL2-mediated macrophages recruitment. Additionally, conditional knockdown of LRP1 in fibroblasts significantly ameliorated psoriasis in mice, suggesting LRP1 as a potential therapeutic target for psoriasis.

2. Materials and methods

2.1. Human specimens

All human studies were authorized by the Institutional Review Board of Ethics at West China Hospital, Sichuan University (Chengdu, China). Normal skin samples were sourced from patients who underwent elective surgeries at West China Hospital, where skin is typically discarded as part of standard procedure. Skin biopsies from patients with active psoriasis were also collected (Approval Number 2019-R-513). Written consents were obtained from all the patients. Additional details about the psoriatic patients are provided in Supporting Information Tables S1 and S2.

2.2. Animals

C57BL/6 mice were acquired from GemPharmatech Co., Ltd. (Nanjing, China). By crossing *Lrp1* floxed mice with *S100a4*-cre

transgenic mice, fibroblast-specific LRP1 knockout mice were generated. These mice were bred and tested at the Experimental Animal Center at Nanjing University of Chinese Medicine (Approval Number: 202206A062). All mice were of the C57BL/6 genetic background, and age- and sex-matched mice aged between 8 and 10 weeks were used. They had free unrestricted access to standard laboratory chow and water, and they were housed in a room with a 12-h light/dark cycle at a constant temperature of 22 °C.

Eighteen healthy cynomolgus monkeys (nine males and nine females, aged between 3 and 5 years) were sourced from the breeding facility of Changchun Biotechnology Development Co., Ltd., Fangchenggang, China. The cynomolgus monkeys were stratified by weight and sex into three groups of 6 cynomolgus monkeys each for this study. The use of cynomolgus monkeys and the experimental procedures were approved by the Changchun Biotechnology Development Animal Ethics Committee (Approval Number: 220071). The monkey management protocols were performed according to the standard protocols of Changchun Biotechnology Development.

2.3. Single-cell RNA sequencing (scRNA-seq) and single-cell ATAC sequencing (scATAC-seq)

The scRNA-seq and scATAC-seq data for this study were generated using the 10 × Chromium platform. The cells were encapsulated into Gel-Bead in Emulsions, where cDNA synthesis took place. Each cDNA molecule within a Gel-Bead in Emulsions was tagged with a consistent 16 nucleotide 10 × barcode and a 12 nucleotide unique molecular identifier (UMI) for library generation. The resulting libraries were then sequenced by Illumina NovaSeq 6000 Sequencing System.

2.4. Generation of data matrix and quality control of scRNA-seq

The raw data of mouse and human were processed by CellRanger v.3.1.0 (10 × Genomics) with the GRCH38 human genome and the mm10−3.0.0 mouse genome as reference. The gene-cell UMI matrices were analyzed using R software (version 3.6.1) for downstream analysis. Low-quality cells were excluded based on filtering criteria that included a UMI count threshold of more than 200 and a mitochondrial gene percentage below 20%.

2.5. Integration of present scRNA-seq data with publicly available data

In order to increase the sample size and enhance the reliability of the analysis results, we integrated our own scRNA-seq data (Normal skin, $n = 3$; Psoriatic skin, $n = 3$) and data from the GEO database. Our scRNA sequencing data have been uploaded to GEO databases (GSE230842). The single-cell sequencing data from the GEO database (GSE173706) was then downloaded[18], including 14 cases of psoriatic skin lesions and 8 cases of normal skin from healthy individuals, and the expression profile of the psoriasis skin microenvironment was mapped by integrating the sequencing data obtained by our sequencing and downloaded from the GEO database. Both datasets were then processed together, including filtering, normalization, and unbiased clustering, with batch effects addressed using appropriate methods.

2.6. Cluster annotation

We used the FindAllMarkers function from the Seurat package to search for the TOP gene in each cluster. We annotate the cell type based on the maker gene in each cluster. To refine our annotations, we referenced marker genes from published literature and combined this with Gene Ontology (GO) functional analysis for each cluster. Additionally, we visualized the expression of these marker genes using the FeaturePlot function as a form of validation.

2.7. Tissue processing and spatial transcriptomics

Placed the skin tissue in a histological plastic box and flash-frozen for 1 min in an isopentane bath cooled with liquid nitrogen. The optimal cutting temperature compound (OCT, Sakura tissue-tek) for subsequently embedding frozen tissue on dry ice. Then we transferred the slices to Visium 10 × 6.5 mm^2 oligomeric barcode capture area on the Visium 10 × Genomics slide. Follow the manufacturer's instructions to perform optimization of the Visium space organization (10 × Genomics). Then follow the manufacturer's instructions (10 × Genomics, Visible Spatial Gene Expression Slide&Reagent Kit) to process sequence libraries.

2.8. Single cell dissociation of skin tissues from human and mouse

Mouse or human tissues were washed in pre-cooled DPBS immediately after isolation. After washing the skin three times with ice-based DPBS, cut the skin to pieces. The skin tissue is then soaked with digestive enzymes (Collagenase I/II and Dispase) at working concentrations. After digestion, place a 70 μm screen on a new 15 mL tube, transfer all to the screen, gently stir the residual tissue on the screen with the gun tip to allow as many cells as possible to pass through the screen, and then add 5 mL DMEM+10% FBS to rinse the screen. If there is redness in the precipitation, 1 × cracking reagent should be used to crack redness: 1 mL 1 × cracking reagent should be added to the cell precipitation, re-mixed, placed on ice for 2−3 min, 5 mL DMEM+10% FBS should be added to terminate the cracking redness, 500 × g at 4 °C, and centrifuged for 5 min. The cells were adjusted to an appropriate number for subsequent experiments.

2.9. Cell−cell interaction

Cell Chat, an important tool that can quantitatively infer and analyze intercellular communication networks from scRNA-seq data based on ligands/receptors among clusters. The compute Commun Prob Pathway function was used to compute the communication probability at the signaling pathway level by summarizing all related ligands/receptors with default parameters. The contribution of each ligand−receptor pair to the overall signaling pathways was computed and visualized using the netAnalysis contribution function.

2.10. Imiquimod (IMQ)-induced psoriasis-like animal model

For the IMQ-induced psoriasis-like mouse model, aged 8−10 weeks C57BL/6 wild-type or transgenic mice were used. Mice received a daily topical application of 62.5 mg of IMQ cream (Aldara; 3M Pharmaceuticals) on their shaved dorsal skin every day for four days. On the day after the last treatment, the mice

were sacrificed. Disease severity was assessed using a clinical Psoriasis Area and Severity Index (PASI) score, ranging from 0 (none) to 4 (very marked), with intermediate score of 1 (slight), 2 (moderate), and 3 (marked). Skin lesions were collected for hematoxylin and eosin (H&E) staining, qPCR analysis, immunofluorescence, and immunocytochemistry.

For the IMQ-induced psoriasis-like Cynomolgus monkey model, eighteen Cynomolgus monkeys (9 males, 9 females) aged 3−5 years were randomly divided into 3 groups: Sham, IMQ, IMQ + CE, the back of the Cynomolgus monkeys were depilated in an area of 3 cm × 3 cm and 120 mg of IMQ cream was applied every morning for 12 days[19]. Two hours after IMQ application, celastrol cream was applied, sham group were treated with vehicle. Skin lesions were collected for H&E staining and immunofluorescence.

2.11. Recombinant mouse IL-23 (rmIL-23)-induced psoriasis-like mouse model

A rmIL-23-induced mouse model of psoriasis was created as previously described[20]. One ear was injected intradermally with 1 μg of rmIL-23 (R&D Systems) dissolved in 25 μL PBS/0.1% BSA, while the contralateral ear received 25 μL PBS/0.1% BSA as a control. Ear thickness was measured daily. Ear lesions were collected for H&E staining and qPCR analysis.

2.12. Quantitative PCR (qPCR)

Total RNA was isolated from mouse skin and ear tissues, as well as from cells (mouse primary skin fibroblasts, peritoneal macrophages), using the RNA Isolater Total RNA Extraction Reagent (Vazyme Biotech Co., Ltd., China). Single-stranded cDNA was synthesized from 1 μg total RNA through reverse transcription. Real-time PCR was conducted on a CFX 100 (Bio-Rad, Hercules, CA, USA) instrument with the primers listed in Supporting Information Table S3. The amplification protocol included an initial denaturation at 95 °C for 2.5 min, followed by 44 cycles of 95 °C for 15 s and 60 °C for 30 s. Dissociation curves were analyzed post-amplification to ensure specificity. Data were normalized to the level of *Gapdh* RNA expression.

2.13. Target discovery via a target-responsive accessibility profiling approach (TRAP)

The identification of celastrol binding proteins was conducted using a previously described method[21]. Treated cells with 100 nmol/L celastrol or DMSO for 1 h, cells followed by permeation and labeling of lysine residues. The lysates were then reduced and alkylated. Desalination, drying, and reconstitution of protein digestates. Analyze the changes in lysine accessibility caused by the binding of celastrol in the sample. The abundance ratio of TRAP-labeled peptides indicated accessibility change and ligand-binding affinity. Using Student's *t*-test, with *P*-value ($P < 0.001$) and *R*-value (TRAP ratio>2 or <0.5) as critical values, evaluate statistical significance to screen celastrol-binding proteins.

2.14. Histological analysis

Dorsal skin tissues from mouse, Cynomolgus monkeys and human were fixed overnight with 4% formaldehyde, embedded in paraffin. Paraffin Sections (5 μm thick) were prepared for H&E staining.

Paraffin sections were deparaffinized, rehydrated, antigen repaired, and blocked, and then incubated overnight at 4 °C with LRP1 primary antibody (Abcam, ab92544) diluted 1:100. For immunohistochemistry, the slides were developed using the DAB kit (Proteintech) according to the manufacturer's instructions.

Immunofluorescence was used to incubate with Alexa Fluor 594-conjugated goat anti-rabbit IgG (H + L) (1:500; Invitrogen, A-11034) and Alexa Fluor 488-conjugated goat anti-mouse IgG (H + L) (1:500; Invitrogen, A-32723) in the dark for 2 h at room temperature. Cell nuclei were stained with DAPI. Use an inverted confocal microscope (Carl Zeiss) to image the sections.

2.15. Immunocytochemistry

Inoculate mouse primary skin fibroblasts at a density of 1×10^5 cells per well in a 24-well culture dish. The cells were fixed, permeabilized, blocked and incubated with anti-LRP1 (Abcam, ab92544) and anti-p-c-Jun (Santa Cruz, sc-822) overnight at 4 °C. Then, the cells were incubated with Alexa Fluor 594-conjugated goat anti-rabbit IgG(H + L) (1:500; Invitrogen, A-11034) and Alexa Fluor 488-conjugated goat anti-mouse IgG(H + L) (1:500; Invitrogen, A-32723) in the dark for 2 h at room temperature. Cell nuclei were stained with DAPI. An inverted confocal microscope (Carl Zeiss) was used to image the sections.

2.16. Western blotting

Lysed cells and determined protein concentrations. Proteins were then separated by SDS-polyacrylamide gel electrophoresis and transferred to polyvinylidene difluoride membranes. The membrane was incubated overnight with primary antibodies, followed by incubation with the second antibody conjugated with horseradish peroxidase. Anti-LRP1 (1:50,000; Abcam, ab92544), anti-p-c-Jun (1:1000; Santa Cruz, sc-822), anti-c-Jun (1:1000; Santa Cruz, sc-74543), anti-p-c-Fos (1:1000; Santa Cruz, sc-81485), anti-c-Fos (1:1000; Santa Cruz, sc-166940), anti-GFP-tag (1:1000; Santa Cruz, sc-9996), anti-Lamin B (1:1000; Proteintech, 12987-1-AP), anti-β-Tubulin (1:2000, Abmart, M20005), anti-β-actin (1:2000, Abmart, M20011), and anti-GAPDH (1:2000, Abmart, M20006) were used.

2.17. MTT assay

Mouse primary skin fibroblasts were inoculated at a density of 5000 cells per well overnight in a 96 well culture dish. The cells were then exposed to varying concentrations of celastrol, prepared in the appropriate cell culture medium, and incubated for 24 h under the same conditions. 20 μL MTT solution was added and the dish was incubated for another 4 h. The medium was removed and each well received DMSO, and the plates were gently agitated to ensure complete solubilization. The absorbance was measured at 570 nm. Compared to untreated control wells, the cell viability was calculated as a percentage. All experiments were conducted in triplicate, with data presented as mean ± standard error of mean (SEM).

2.18. Cellular thermal shift assay (CETSA)

CETSA was conducted as previously described[22]. Mouse primary skin fibroblasts were divided into two groups: one treated with 100 nmol/L celastrol and the other serving as a control with an

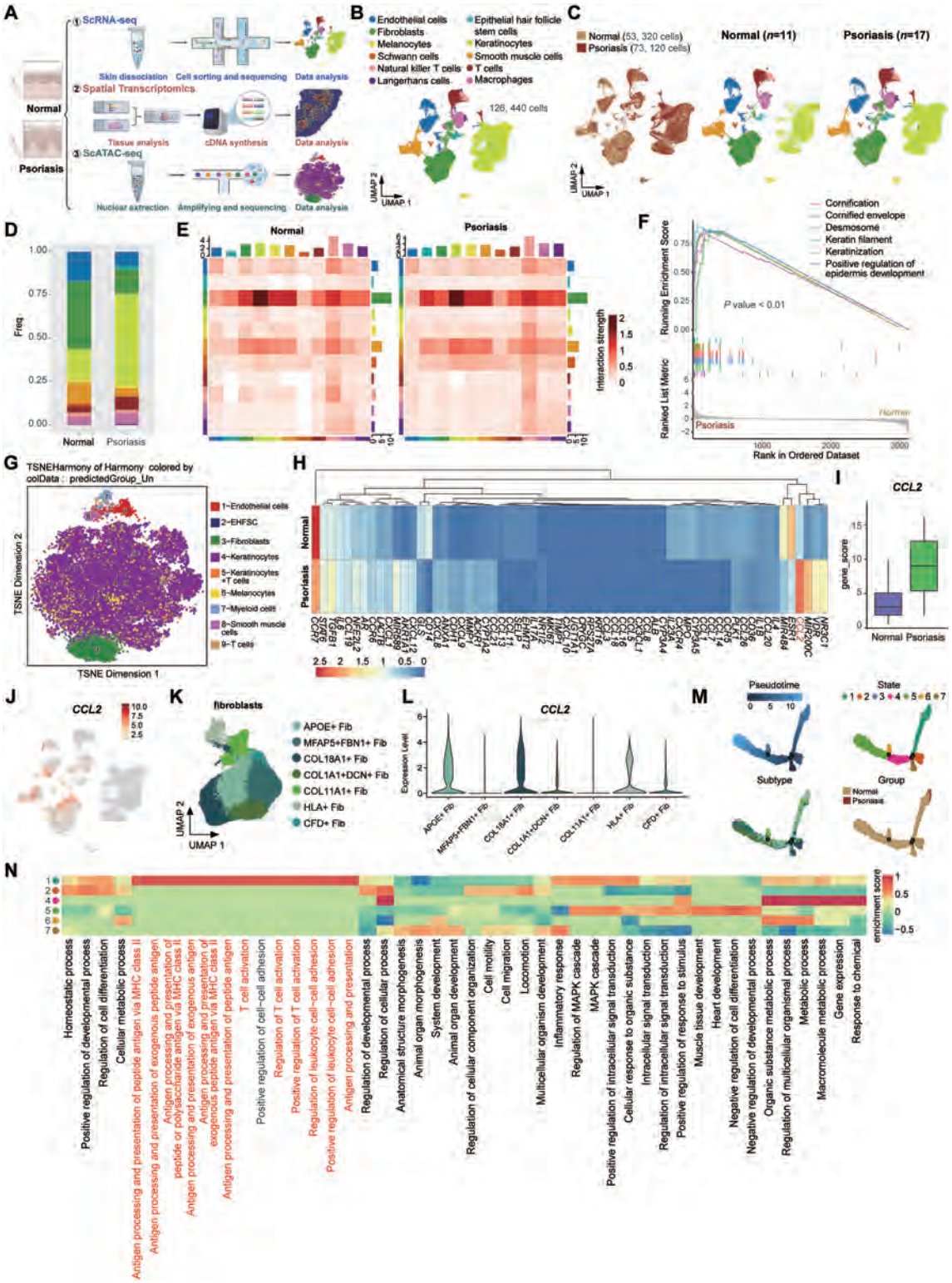

Figure 1 Single-cell multi-omics reveals fibroblasts' importance in psoriasis. (A) Schematic diagram of single-cell transcriptomics, spatial transcriptomics, and scATAC-seq studies in normal individuals and psoriatic patients' skin. (B, C) UMAP of scRNA-seq cells recovered from 11 normal individuals and 17 psoriatic patients (GEO databases: GSE230842 and GSE173706). (D) Proportional map of each cell subpopulation in skin tissue of psoriasis patients and normal individuals. (E) Strength of interactions between skin cell types of normal individuals (*left*) and psoriasis patients (*right*). (F) GSEA enrichment analysis of psoriasis-related terms. (G) T-SNE plot showing the joint clustering of scATAC-seq data in skin tissues. Cells in the T-SNE are annotated by scRNA-seq data T-SNE plots colored by clusters, labeled by scRNA-seq data. (H) The heatmap showing the gene expression and chromatin accessibility of CCL family genes in fibroblasts of psoriasis patients and normal individuals skin tissues. (I) Expression Gene score of *CCL2* in skin tissues of psoriasis patients and normal individuals. Based on scATAC-seq data. (J)

equivalent volume of DMSO. After 2 h, the cells were washed and resuspended in PBS. Both groups were then divided into eight 50 μL aliquots and transferred into PCR tubes. The PCR machine was set to generate 8 temperature gradients (52, 55, 58, 61, 64, 67, 70, and 73 °C). Each aliquot in the control group was assigned to a specific temperature, and the corresponding aliquot in the treatment group was subjected to the same temperature, heated for 3 min, then cooled for 3 min, and then placed in an ice bath. After processing all samples, they were freeze−thawed: placed overnight in a −80 °C freezer, thawed at room temperature, refrozen for 2 h, and repeated this cycle twice. The processed samples were centrifuged at 20,000 × *g* for 20 min, mixed with 6-fold loading buffer, heated for 5 min, and analyzed by SDS-polyacrylamide gel electrophoresis.

2.19. Microscale thermophoresis (MST)

HEK293T cells were transfected with EGFP-LRP1^{wt}, EGFP-LRP1^{mut1}, EGFP-LRP1^{mut2}, and EGFP-LRP1^{mut3} plasmids. After 48 h, the cells were lysed and centrifuged. Each ligand diluent was incubated with an equal volume of cell lysate for 10 min, then transferred to zero-background capillaries and measured using a Monolith NT.LabelFree instrument (NanoTemper Technologies). MO.Affinity Analysis v2.3 software as used to analyze the data from at least three independent measurements.

2.20. RNA interference

Small interfering RNA (siRNA) targeting mouse *Lrp1* was synthesized by GenePharma: 1# sense: CCACCUGCUAUGAGUU UAATT, antisense: UUAAACUCAUAGCAGGUGGTT; 2# sense: GCCCAUUGGAUGAGUUUCATT, antisense: UGAAAC UCAUCCAAUGGGCTT; 3# sense: GCGUGGUGUUCUGGUA UAATT, antisense: UUAUACCAGAACACCACGCTT. The transfection of siRNA was performed using the Hieff Trans® *in vitro* siRNA/miRNA Transfection Reagent (Yeasen Biotechnology (Shanghai) Co., Ltd.).

2.21. Cytoplasm and nuclear protein separation

Buffer A and NP-40 were added to lyse cells, and vortexed periodically over 30 min. After centrifugation at 12,000 × *g* for 10 min, the supernatant was cytoplasm. Cell pellet was lysed by RIPA, and centrifuged again at 12,000 × *g* for 10 min. The supernatant obtained was the nuclear fraction. The samples were mixed with 6-fold loading buffer, heated for 5 min, and subjected to Western blotting analysis.

2.22. Statistical analysis

Statistical analysis was performed using GraphPad Prism 9.0. The data were presented in the form of mean ± SEM. We evaluated the normal distribution and homogeneity of variance across groups of data. The unpaired two-tailed Student's *t*-tests and Tukey's multiple comparisons test were used to determine statistical significance (*$P < 0.05$, **$P < 0.01$, ns = not significant).

3. Results

3.1. Single-cell multi-omics reveals fibroblasts' importance in psoriasis

To investigate the skin microenvironment of psoriatic patients, we integrated single-cell sequencing data from GSE173706 and our group, including 17 cases of skin lesions from psoriatic patients and 11 cases of skin tissues from healthy individuals (*e.g.*, circumcision samples) (Fig. 1A). First, we performed quality control on the sequencing data and then proceeded to the subsequent analysis (Supporting Information Fig. S1). The uniform manifold approximation and projection (UMAP) plots showed the integration of the two groups (Fig. 1B) and the subpopulations of cells clustered separately (Fig. 1C), which contained 11 clusters of cells—namely, endothelial cells, epithelial hair follicle stem cells, fibroblasts, keratinocytes, melanocytes, smooth muscle cells, Schwann cells, T cells, natural killer T cells, macrophages, and Langerhans cells (Supporting Information Table S4). The expression levels of the differentially expression genes are shown in Supporting Information Fig. S2. Based on the proportional map of cell proportions, keratinocytes and fibroblasts accounted for a high proportion (Fig. 1D), and the interaction of fibroblasts with immune cells, especially macrophages, was significantly increased in psoriasis patients (Fig. 1E). Gene set enrichment analysis (GSEA) comparing psoriasis to the normal group revealed psoriasis biological traits related to keratinocytes, such as cornification and keratin filaments (Fig. 1F). We were more concerned about whether a large number of fibroblasts are involved in the progression of psoriasis and what role they play in this process. We also performed scATAC-seq on the skin lesions of psoriasis patients and healthy individuals, gathered quality control on sequencing data (Supporting Information Fig. S3), and then established a scATAC-seq atlas (Fig. 1G, Supporting Information Fig. S4). *CCL2* expression was substantially increased in the skin lesions of psoriatic patients compared to healthy individuals (Fig. 1H and I, Supporting Information Fig. S5). We then analyzed the expression of the chemokine CC family in various cell subpopulations; notably, *CCL2* was predominantly expressed in fibroblasts (Fig. 1J, Supporting Information Fig. S6). In general, the chemokine CCL2 activated and recruited monocytes/macrophages to the inflammatory areas mainly by recognizing and binding to its specific receptor CCR2 during the onset of inflammation[23−25].

We then divided the fibroblasts into APOE$^+$, MFAP5$^+$FBN1$^+$, COL18A1$^+$, COL1A1$^+$DCN$^+$, COL11A1$^+$, HLA$^+$, and CFD$^+$ fibroblasts (Fig. 1K, Supporting Information Fig. S7A), with *CCL2* mainly distributed in the subpopulation of HLA $^+$ fibroblasts (Fig. 1L), which was mostly present in the psoriasis group (Fig. S7B). According to the results of GO analysis of the pseudotime trajectory, HLA $^+$ fibroblasts subpopulations with high expression of *CCL2* were associated with T-cell activation and macrophage function (Fig. 1M and N, Fig. S7C). We hypothesize that HLA$^+$ fibroblasts exacerbate psoriasis progression by recruiting macrophages through CCL2 secretion.

Expression of *CCL2* on scRNA-seq data. (K) Distribution of fibroblast subtype on the UMAP. (L) VlnPlot showing the expression of *CCL2* in each fibroblast subtype. (M) Pseudotime trajectory of fibroblast subtypes visualized using Monocle2. The trajectory is color-coded from left to right by pseudotime, cell states, subtypes, and groups. (N) Heatmap displaying the functional pathways that are both highly and poorly enriched in the six cell states of fibroblast subtypes, as determined by GSEA. **P value < 0.01.

3.2. *Ccl2 inhibition improves psoriasis-like skin inflammation in mice*

We screened 1896 natural small-molecule compounds and found that celastrol prominently inhibited *Ccl2* expression in fibroblasts with a 97% inhibition rate (Fig. 2A and B). To evaluate the ameliorative effect of celastrol on psoriasis, we administered celastrol treatment to mice with psoriasis. Celastrol significantly improved the erythema and scaling of mouse skin, inhibited epidermal thickening and infiltration of inflammatory cells

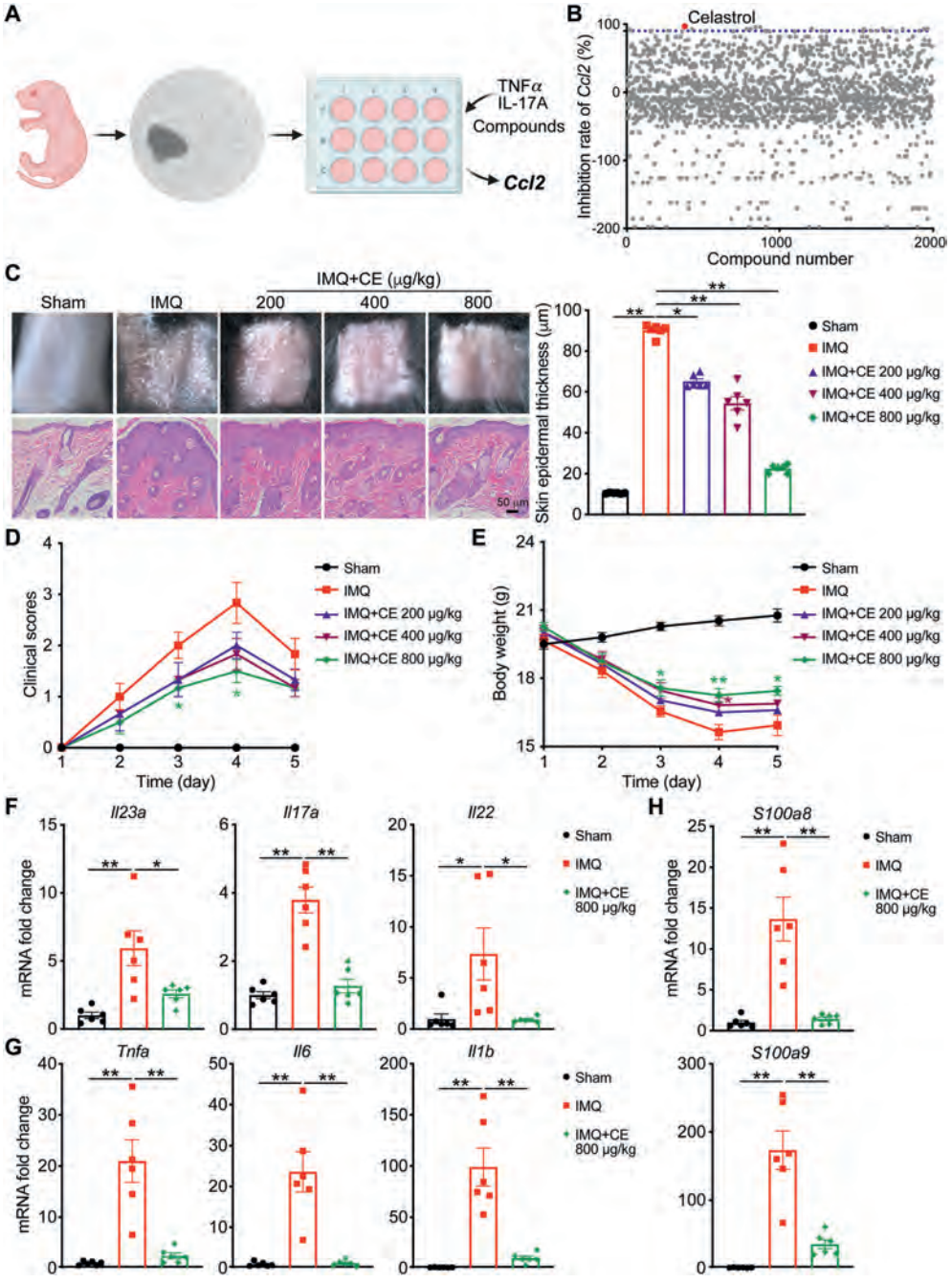

Figure 2 *Ccl2* inhibition improves imiquimod-induced psoriasis-like skin inflammation in mice. (A, B) The process for screening of *Ccl2* inhibitors. Primary skin fibroblasts derived from C57BL/6 mice, untreated or pre-treated with 1896 natural small molecule compounds (MedChemExpress, Library ID: HY-LD-000004273) and then stimulated by TNFα and IL17A for 6 h qPCR analysis of *Ccl2* mRNA expression. The blue dotted line represents the 90% inhibition threshold. Celastrol is labelled, and inhibited *Ccl2* expression by 97.0%. C57BL/6 female mice (n = 6/group) were treated intraperitoneally with the indicated doses of celastrol (CE) for four days (C−H). (C) Phenotypic representation (*top*) and H&E staining (*bottom*) of back skin sections of Sham, IMQ-induced and celastrol-treated mice. Skin epidermal thickness statistics for each group on the *right*. (D) Clinical scores of Sham, IMQ-induced and celastrol-treated mice. (E) Body weight during the disease process. (F−H) qPCR analysis of mRNA encoding cytokines from the IL-23/Th17 cell axis (F), pro-inflammatory cytokines (G), and keratin formation-related cytokines (H) in the skin. The Data are represented as mean ± SEM. The P-values are determined by a two-tailed unpaired Student's t-test for (C, F−H) or Tukey's multiple-comparison test for (D, E). $^*P < 0.05$, $^{**}P < 0.01$.

(Fig. 2C, Supporting Information Fig. S8), reduced clinical scores (Fig. 2D), and slowed down the decrease in body weight of the mice (Fig. 2E). Celastrol did not affect the skin condition of normal mice (Supporting Information Fig. S9). Administration of high doses of celastrol distinctly reduced the expression levels of the "IL-23/Th17 cell axis" gene (Fig. 2F), inflammation-related genes (Fig. 2G) and keratin formation-related genes (Fig. 2H). Celastrol also showed improved effects on rmIL-23-induced psoriasis (Supporting Information Fig. S10). These data demonstrate that celastrol ameliorated the progression of psoriasis induced by IMQ and rmIL-23 in mice.

To verify the important role of CCL2 in psoriasis, we treated psoriasis-like mice with CCL2 neutralizing antibodies and found that anti-CCL2 significantly improved the psoriasis like phenotype induced by IMQ in mice. We also found that the administration of celastrol on the addition of this treatment did not further improve the disease (Supporting Information Fig. S11), suggesting that celastrol ameliorates psoriasis in mice by inhibiting CCL2.

3.3. The scRNA-seq analysis demonstrates that celastrol blocks fibroblast-myeloid cell crosstalk in mice

We applied the single-cell sequencing technique to mouse psoriasis. Firstly, 800 μg/kg of celastrol was administered to C57BL/6 mice (similar to Fig. 2), which significantly improved the development of psoriasis in the mice (Supporting Information Fig. S12). Next, the dorsal skin of mice in the normal control, imiquimod-induced and celastrol-administered groups was taken, cut, digested by digestive enzymes and prepared into single-cell suspensions for 10× genomics single-cell transcriptome sequencing (Fig. 3A). UMAP plots were obtained by nonlinear dimensionality reduction using Seurat, where each point in the plot represented a cell, and cells with similar expression characteristics were spatially located close together, with different colors representing different cell subpopulations. The cell populations were annotated according to the Top 30 differentially expressed genes in each cluster of cells, combined with the Cell Marker website and a review of the literature, including fibroblasts, lymphocytes, myeloid cells, Schwann cells, keratinocytes, smooth muscle cells and endothelial cells (Fig. 3B and C). Dot plots demonstrate the expression levels of differentially expressed genes (Fig. 3D). UMAP plots show the expression levels of marker genes in the cell groups (Fig. 3E). Marker genes demonstrates the accuracy of cell annotation. Occupancy analysis of the cell groups showed the highest percentage of fibroblasts (Fig. 3F). GO analysis confirmed the function of each cluster (Supporting Information Fig. S13). We performed KEGG analysis on fibroblasts in the skin lesions of three groups of mice and found that the cytokine-mediated signaling pathway and the regulation of inflammatory response were obviously upregulated in the model group and could be significantly downregulated after celastrol administration (Supporting Information Fig. S14). Cellular interaction analysis revealed that the CCL signaling pathway was significantly inhibited in the communication between fibroblasts and myeloid cells after celastrol treatment (Fig. 3G, Supporting Information Fig. S15), and *Ccl2* was mainly expressed in fibroblasts (Fig. 3H). Spatial transcriptome sequencing analysis on normal skin and psoriatic patients' lesions was performed, with quality control on the sequencing data shown in Supporting Information Fig. S16. *CCL2* was distributed in psoriasis patients' lesions significantly more than in normal individuals (Fig. 3I), and consistently, *Ccr2* expression was significantly higher in the model group, and celastrol treatment significantly inhibited the expression of *Ccr2* (Fig. 3J). Furthermore, dorsal skin lesion tissues from sham, model, and celastrol-administered mice were taken to assess the expression levels of chemokines and their receptors. Notably, both *Ccl2* and *Ccr2* were found to be highly expressed in the model group. Celastrol administration resulted in a significant reduction of their mRNA levels (Fig. 3K). In addition, celastrol also inhibited the expression of CCL2 in the skin lesions' fibroblasts (Supporting Information Fig. S17A) and serum (Fig. S17B) of IMQ-induced mice. Further analysis of myeloid cells revealed that celastrol had an inhibitory effect on their function (Supporting Information Fig. S18).

3.4. Celastrol targets LRP1 to alleviate psoriasis in mice

How does celastrol affect fibroblasts? First, we examined the effect of celastrol on the proliferation of mouse primary skin fibroblasts, and 1 μmol/L celastrol was cytotoxic (Fig. 4A). Since TNFα and IL17A are highly expressed in the inflammatory microenvironment of psoriatic skin, we administered these to the primary fibroblasts, and because 300 nmol/L celastrol was cytotoxic (Fig. 4B), the maximum concentration of celastrol in the follow-up experiments was 100 nmol/L. The target binding accessibility profile TRAP assay identified LRP1, a candidate target protein for celastrol (Fig. 4C). LRP1 is described as a 600 kDa type I glycosylated transmembrane protein which belongs to the LDL receptor gene family[26] consisting of a 515 kDa N-terminal extracellular domain (α chain) containing ligand-binding regions and an 85 kDa membrane-anchored C-terminal intracellular domain (β chain)[27]. Single-cell transcriptome sequencing analysis of skin tissues from psoriatic patients and healthy individuals revealed that LRP1 was predominantly expressed in the fibroblasts (Fig. 4D), and spatial transcriptome sequencing data showed that the expression level of LRP1 was obviously higher in psoriasis patients' skin lesions than in healthy individuals (Fig. 4E), as evidenced by immunohistochemical experiments (Fig. 4F). Similarly, *Lrp1* was highly expressed in the skin lesions of IMQ induced psoriasis like mice compared with the sham group, and celastrol reduced *Lrp1* expression (Fig. 4G). Cellular thermal shift assays demonstrated the *in vivo* binding of celastrol to LRP1 (Fig. 4H). Then, we verified the *in vitro* binding of celastrol to LRP1 by pull down assay with the help of a biotin probe labeled celastrol (Fig. 4I), and the binding was also confirmed by immunofluorescence (Fig. 4J). Further, with the use of molecular docking experiments, we found that celastrol could bind at the 3989, 3972, and 4161 sites of LRP1, located in the LRP1 β chain. Therefore, we constructed an LRP1 85 kDa plasmid ($LRP1^{wt}$) with an EGFP tag and demonstrated the binding of celastrol to LRP1 by microscale thermophoresis (MST) with a binding affinity of 99.6 nmol/L (Fig. 4K and L), consistent with the dose used on cells. We also constructed mutation plasmids mutated to alanine at the 3989, 3972, and 4161 sites of LRP1, respectively, corresponding to $LRP1^{mut1}$, $LRP1^{mut2}$, and $LRP1^{mut3}$, respectively, and the MST results showed that the $LRP1^{mut2}$ corresponding site could be the key binding amino acid. Next, we tested whether LRP1 affects *Ccl2* transcription, so small interfering RNA of *Lrp1* (si-*Lrp1*) and LRP1 plasmids were constructed and tested for their efficiency in mouse primary skin fibroblasts (Fig. 4M and N), with the most efficient interference of si-*Lrp1* #2, and the second one was used for all the subsequent knockdown experiments. TNFα and IL17A increased *Ccl2* expression, while the administration of celastrol treatment decreased its expression. Consistently, the knockdown of LRP1 also decreased its

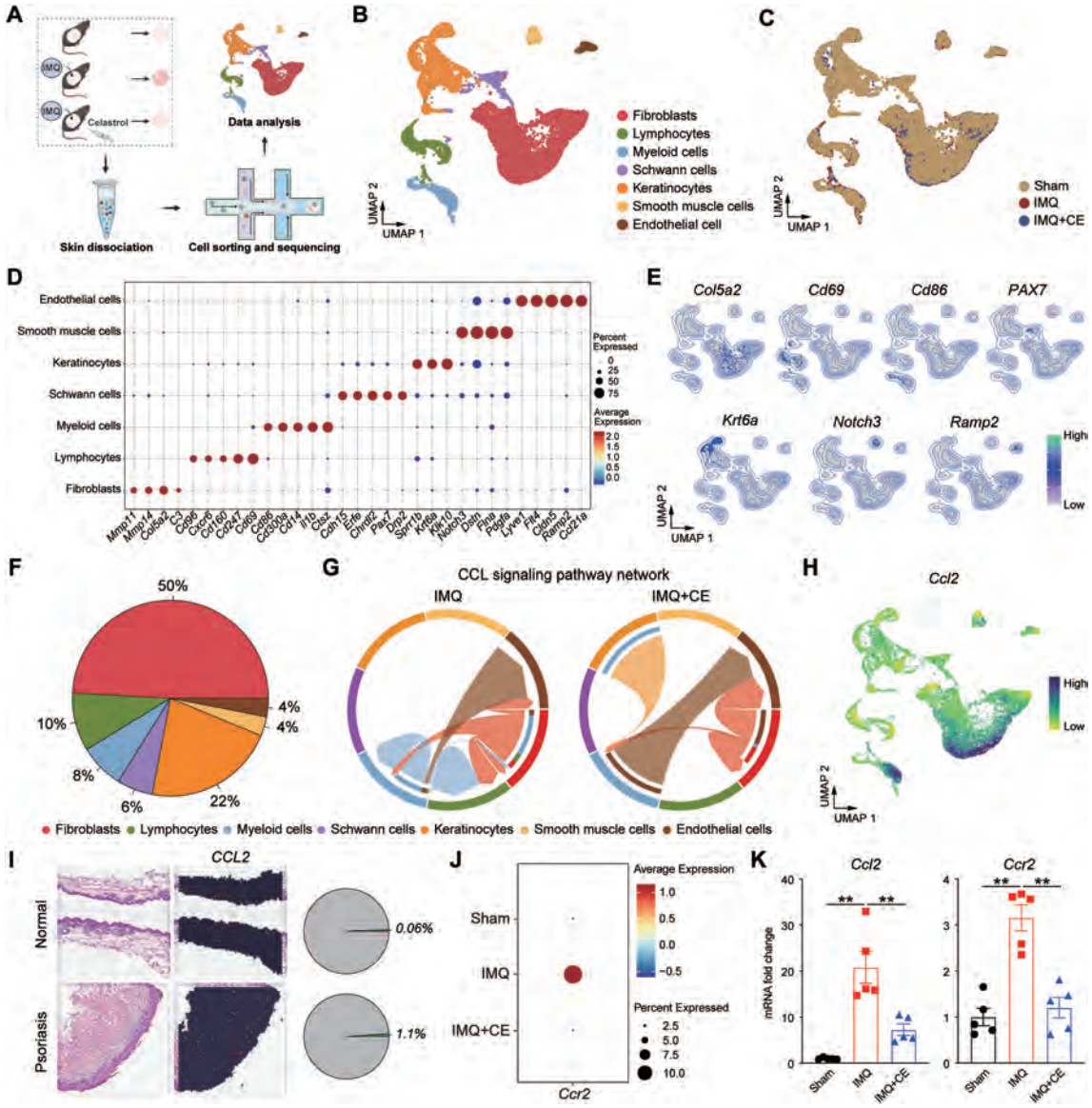

Figure 3 The scRNA-seq analysis demonstrates that celastrol blocks fibroblast-myeloid cell crosstalk in mice. (A) Workflow of dorsal skin scRNA-seq analysis for Sham, IMQ, and IMQ + CE groups. (B, C) UMAP of scRNA-seq cells recovered from Sham, IMQ and IMQ + CE groups. (D) Dot plot for expression of marker genes in skin cell types. (E) Projection of gene expression of known cell type specific markers across cell groups. (F) Proportional map illustrating the distribution of each cell subpopulation within the skin tissue of the Sham, IMQ, and IMQ + CE groups. (G) Number of interactions between IMQ induced C57BL/6 mouse skin cell types, untreated (*left*) or treated with CE (*right*). (H) Expression of *Ccl2* in skin cell types. (I) Spatial distribution and proportion of *CCL2* in psoriasis patients and normal individuals skin tissues. (J) *Ccr2* expression in Sham, IMQ, and IMQ + CE groups. (K) Expression of *Ccl2* and *Ccr2* in Sham, IMQ and IMQ + CE groups. The data are represented as mean ± SEM. The *P*-values are determined by two-tailed unpaired Student's *t*-test. $^{**}P < 0.01$.

expression, while the overexpression of LRP1 significantly elevated the expression level of *Ccl2* (Fig. 4O and P), showing that LRP1 can positively regulate the transcription of *Ccl2*.

3.5. Celastrol prevents LRP1 from binding with c-Jun

Since LRP1 regulates the transcription of *Ccl2*, we used scATAC-seq to determine whether celastrol affects the transcription factor (TF) function of *Ccl2* by targeting LRP1, thereby inhibiting its transcription. We analyzed scATAC-seq data from the skin of psoriatic patients and normal individuals, ranking TF according to their importance in fibroblasts, and found that the AP-1 components FOS and JUN were significantly enriched (Fig. 5A). Next, CXCL family-related genes were analyzed for differential expression in psoriasis patients' and normal individuals' skin tissues, and *JUN* was significantly upregulated in patient lesions (Fig. 5B). Mapping the genome tracks of psoriatic patients' skin lesions did not reveal that peaks fell within the region of *JUN*, indicating a high degree of *JUN* accessibility (Fig. 5C). The administration of TNFα and IL17A stimulation to primary mouse skin fibroblasts significantly elevated

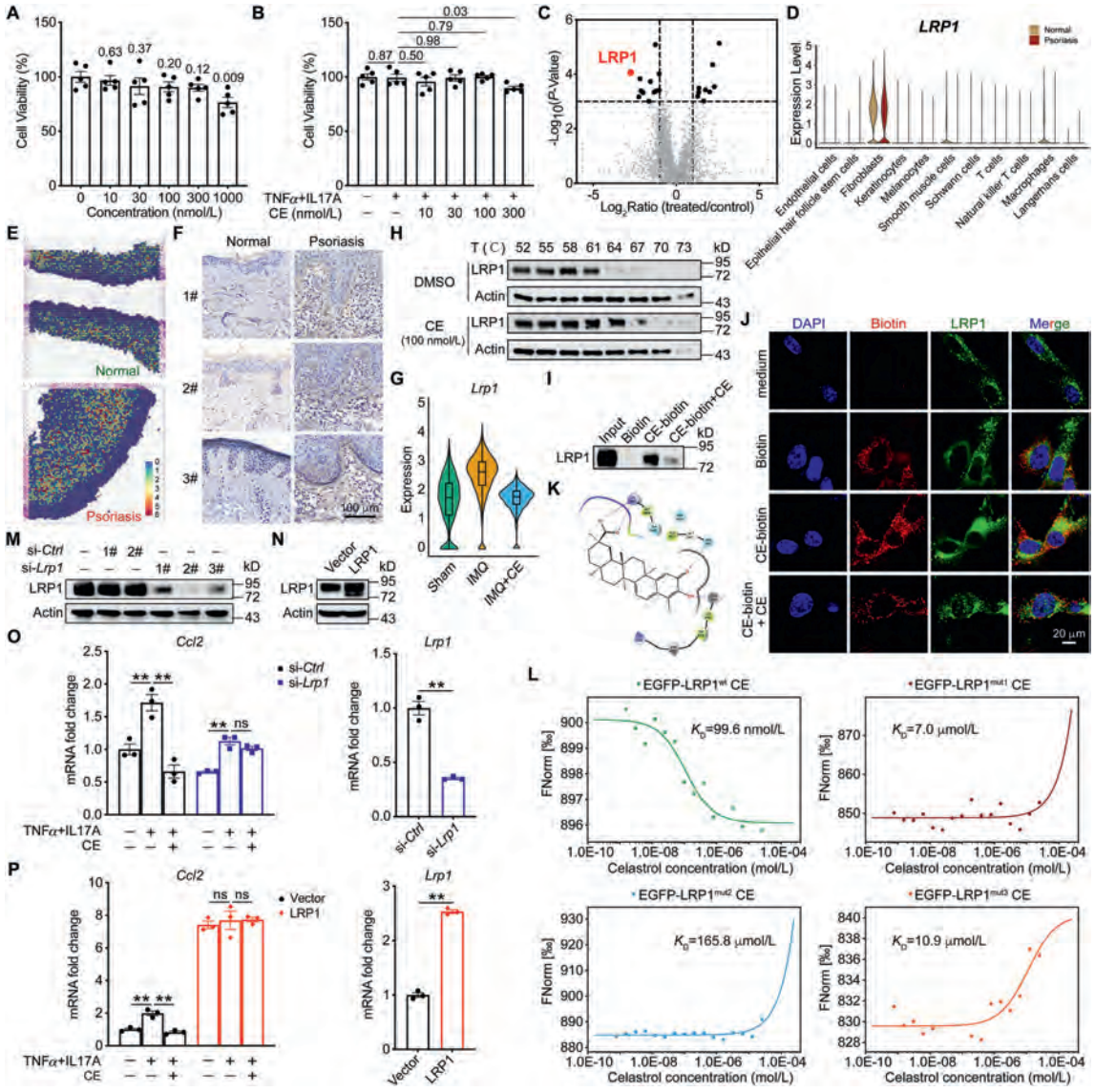

Figure 4 Celastrol targets LRP1 to alleviate psoriasis in mice. (A, B) Mouse primary skin fibroblasts were analyzed using MTT assay. (C) Celastrol directly binding proteins using TRAP assay. (D) *LRP1* expression in various cell populations of the scRNA-seq of psoriasis patients and normal individuals skin tissues. (E) Spatial feature plot of *LRP1*'s expression. (F) LRP1 staining in skin sections of psoriatic patients ($n = 3$) and normal individuals ($n = 3$). (G) Expression of *Lrp1* in skin tissue from Sham, IMQ and IMQ + CE groups. (H−L) Binding of celastrol to LRP1 was detected using CETSA (H), pull down (I), immunofluorescence (J), docking (K), and MST (L). (M, N) LRP1 expression in mouse primary skin fibroblasts infected with si-*Ctrl*, si-*Lrp1*, vector, or LRP1 plasmids. (O, P) qPCR detection of mRNA expression of *Ccl2* and *Lrp1* in knockdown (O) and overexpression (P) LRP1 mouse primary skin fibroblasts. The data are represented as mean ± SEM. The *P*-values are determined by Tukey's multiple comparison test for (O, P). $^*P < 0.05$, $^{**}P < 0.01$.

the phosphorylation level of c-Jun, which was reduced by celastrol treatment. Similarly, knockdown of LRP1 significantly suppressed p-c-Jun levels (Fig. 5D), while overexpression of LRP1 promoted c-Jun phosphorylation (Fig. 5E). TNFα and IL17A promoted LRP1 nuclear translocated into the, and administration of celastrol inhibits LRP1 nuclear translocation (Fig. 5F). As a transcription factor, c-Jun binds to the promoter region of the *Ccl2* and activates its transcription[28,29]. Next, we overexpressed the LRP1 in HEK293T cells, and immunoprecipitation experiments demonstrated that celastrol inhibited the binding of LRP1 to c-Jun in the nucleus (Fig. 5G), which was corroborated by immunofluorescence experiments (Fig. 5H, Supporting Information Fig. S19). Therefore, we suggest that celastrol targeting LRP1 prevents its binding to c-Jun in the nucleus and thus inhibits CCL2 production by fibroblasts.

3.6. LRP1 deficiency relieves the IMQ-induced psoriasiform inflammation

To further define the role of LRP1 in psoriasis progression, we crossed *Lrp1*$^{flox/flox}$ mice with *S100a4*-cre mice and constructed fibroblasts-specific LRP1 conditional knockout mice, and confirmed the efficiency of *Lrp1* deletion in mouse primary skin fibroblasts (Supporting Information Fig. S20). We administered imiquimod to the dorsal skins of the wild-type and *Lrp1*$^{-/-}$ mice.

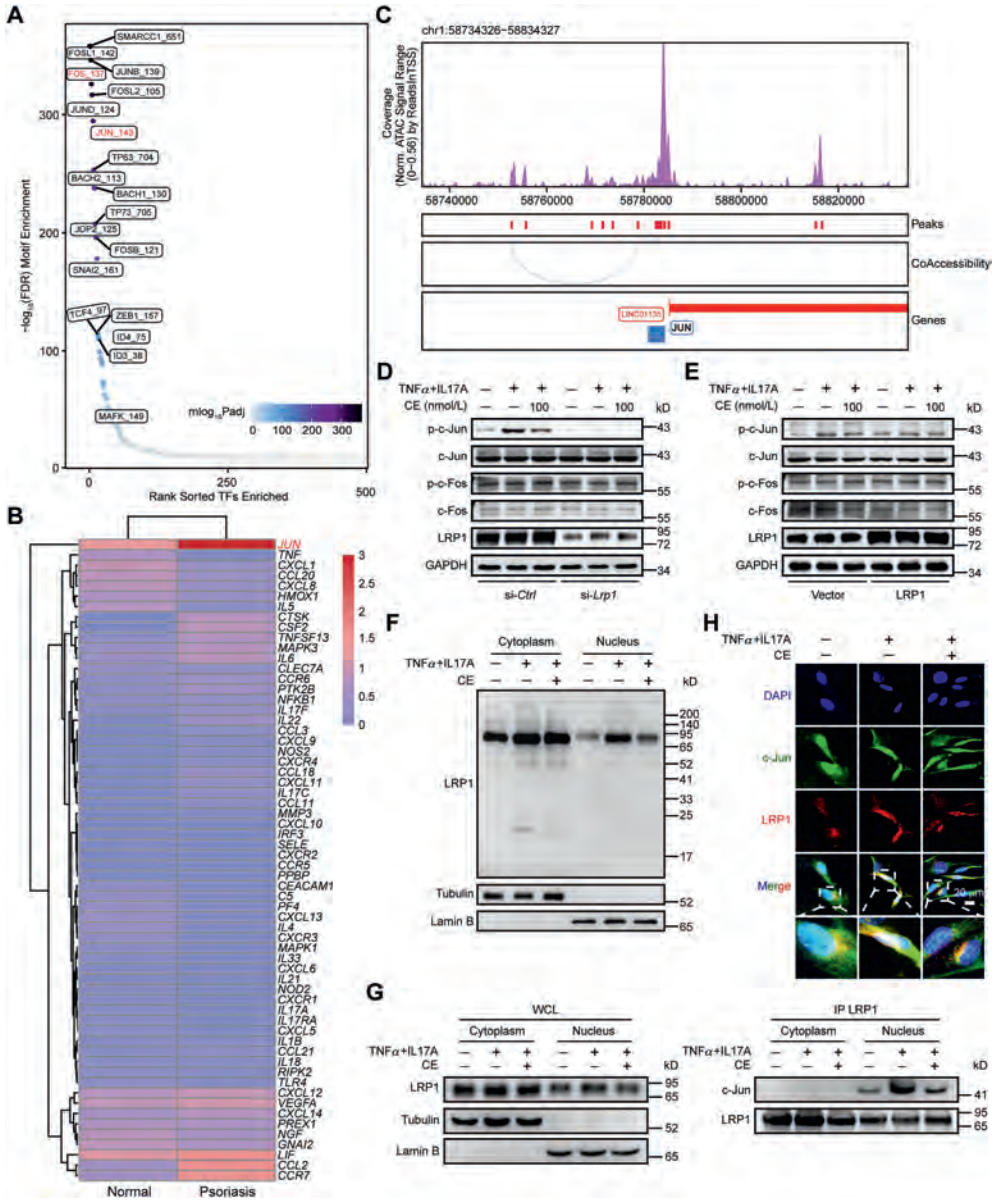

Figure 5 Celastrol prevents LRP1 from binding with c-Jun. (A) Plot of rank-sorted TF motifs and colored by the significance of their enrichment in fibroblasts, which compared the psoriasis group with the normal group and based on the scATAC-seq profiles. (B) Heatmap of CXCL family -related genes in each group. (C) Genome tracks of JUN in psoriasis group. (D, E) Phosphorylation levels of transcription factors c-Jun and c-Fos in knockdown (D) and overexpression (E) of LRP1 mouse primary skin fibroblasts. (F) Mouse primary skin fibroblasts derived from C57BL/6 mice were stimulated by TNFα and IL17A and treated with or without celastrol. Conducted subcellular separation and detect cytoplasm and nuclear proteins with respective antibodies. (G) Fibroblasts were stimulated by TNFα and IL17A and treated with or without celastrol, followed by isolation of the cytoplasm and nucleus and immunoprecipitation using anti-LRP1 beads. (H) Immunofluorescence staining of primary skin fibroblasts generated from C57BL/6 mice was stimulated by TNFα and IL17A and treated with or without celastrol. Scale bar: 20 μm.

The *Lrp1*$^{-/-}$ mice exhibited significant improvements in psoriasis-like phenotype compared to their wild-type counterparts, including reduced erythema and scaling (Fig. 6A), decreased epidermal thickness and inflammatory cells infiltration (Fig. 6B and C), lower clinical scores (Fig. 6D), and improved body weight (Fig. 6E). Furthermore, in the skin of *Lrp1*$^{-/-}$ mice treated with IMQ, IL-23/Th17 cell axis related genes (Fig. 6F) and other pro-inflammatory cytokines (Fig. 6G) expression were markedly reduced. LRP1 deficiency also inhibited the expression of CCL2 in the dorsal skin (Supporting Information Fig. S21). Knockdown of *Lrp1* in fibroblasts caused a decrease in c-Jun entry into the nucleus (Fig. 6H). By analyzing cellular interactions in skin lesions from psoriasis patients and IMQ-induced psoriasis-like changes in mice revealed enhanced communication between fibroblasts and myeloid cells. Since the group previously had more and stronger fibroblast-macrophage communication in the dermis of psoriatic patients' skin lesions[30], so we investigated whether LRP1 deficiency affected the production of psoriasis-related inflammatory factors by macrophages. Knockdown of *Lrp1* in fibroblasts or administration of fibroblasts with celastrol resulted

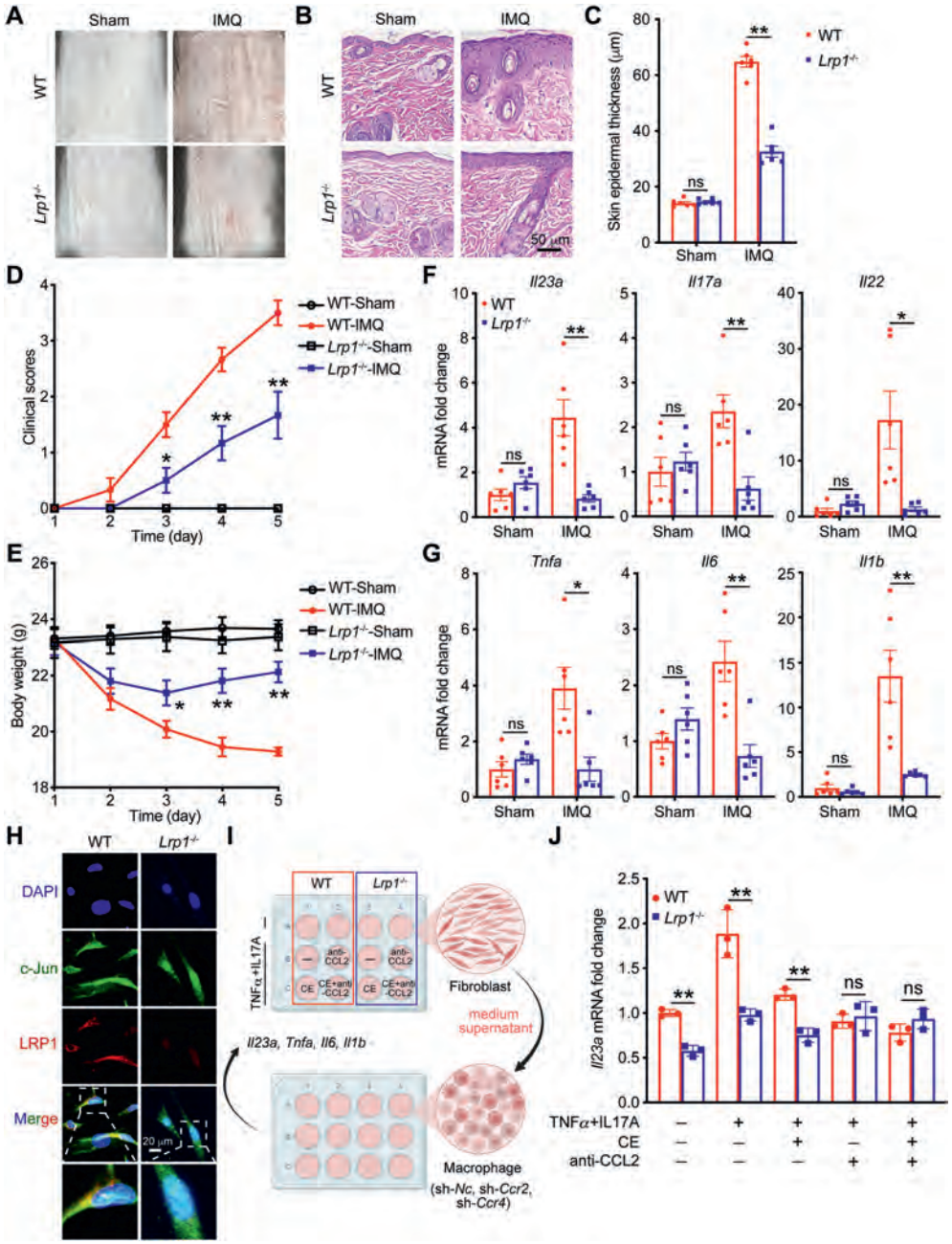

Figure 6 LRP1 deficiency relieves the IMQ-induced psoriasiform inflammation. (A−E) Phenotypic representation (A), representative H&E staining (B), epidermal thickness (C), clinical scores (D), and body weight (E) of back skin sections of wild-type (WT) ($n = 6$) and *Lrp1*$^{-/-}$ mice ($n = 6$) treated with IMQ for 4 days. (F, G) qPCR analysis of mRNA encoding cytokines from the IL-23/Th17 cell axis (F) and pro-inflammatory cytokines (G) in skin. (H) Immunofluorescence staining of primary skin fibroblast generated from *Lrp1*$^{-/-}$ mice and wild-type mice. Scale bar: 20 μm. (I) Diagram of cell co-culture model. Primary skin fibroblasts derived from *Lrp1*$^{-/-}$ and wild-type mice were pre-treated with celastrol and then stimulated by TNFα and IL17A, and the cell culture supernatants were co-cultured with mouse peritoneal macrophages (sh-*Nc* or sh-*Ccr2* or sh-*Ccr4*) for 6 h. (J) Primary skin fibroblasts derived from *Lrp1*$^{-/-}$ and wild-type mice were pre-treated with celastrol, anti-CCL2, or both celastrol and anti-CCL2, and then stimulated by TNFα and IL17A for 1 h, and removed them. After another 24 h of incubation, the cell culture supernatants were co-cultured with mouse peritoneal macrophages for 6 h to detect the mRNA expression of psoriasis-related factors in peritoneal macrophages. Results were normalized to *Gapdh* expression. The data are represented as mean ± SEM. The *P*-values are determined by Tukey's multiple comparison test for (C−G, J). $^{*}P < 0.05$, $^{**}P < 0.01$, ns, not significant.

in reduced expression of psoriasis-related inflammatory factors in macrophages (Fig. 6I and J, Supporting Information Fig. S22). The absence of LRP1 and treatment with celastrol or CCL2 neutralizing antibodies both inhibited the production of psoriasis-related inflammatory factors by macrophages (Fig. S22). However, if macrophages lacked *Ccr2* (Supporting Information Fig. S23) or *Ccr4* (Supporting Information Fig. S24), the aforementioned effects caused by the LRP1 deficiency in the fibroblasts disappeared. Thus, celastrol inhibits macrophage function and ameliorates psoriasis by targeting LRP1 in fibroblasts.

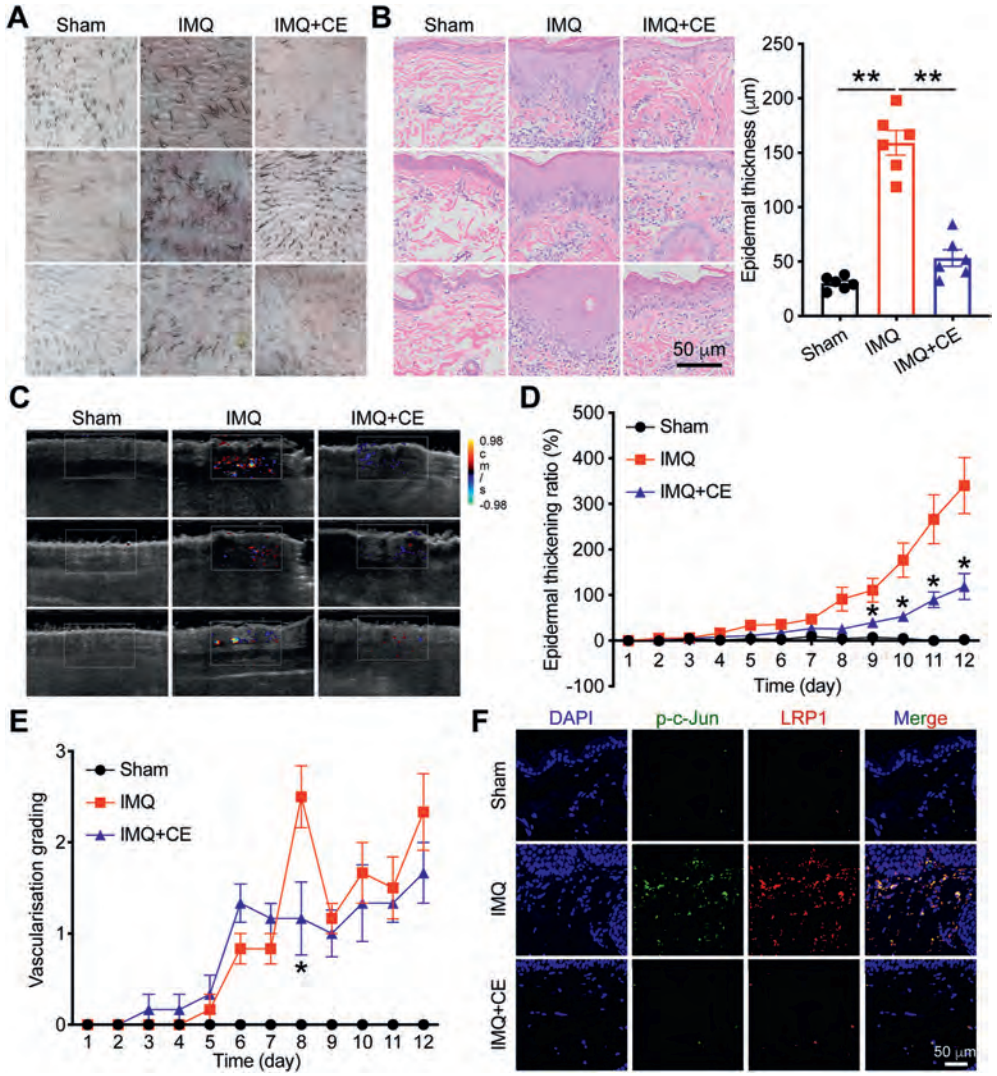

Figure 7 Celastrol ameliorates psoriasis-like inflammation in cynomolgus monkeys. Cynomolgus monkeys (n = 6/group) were applied with celastrol on the back for 12 days. (A, B) Phenotypic representation (A) and representative H&E staining (B) of back skin sections of Sham, IMQ-induced, and celastrol-treated Cynomolgus monkeys. Scale bar: 50 μm. (C) Ultrasound imaging of Cynomolgus monkey skin. (D) Epidermal thickening ratio of Cynomolgus monkeys during the disease process. (E) Cynomolgus monkey skin vascularisation grading. (F) Skin sections from Sham, IMQ-induced, and celastrol-treated Cynomolgus monkeys were immune-stained for LRP1 together with p-c-Jun. Scale bar: 50 μm. The data are represented as mean ± SEM. The P-values are determined by Tukey's multiple comparison test for (B, D, E). *$P < 0.05$, **$P < 0.01$.

3.7. Celastrol ameliorates psoriasis-like inflammation in cynomolgus monkeys

To assess the translational potential of celastrol for the treatment of psoriasis, we induced psoriasis-like skin inflammation by applying IMQ to the dorsal skin of cynomolgus monkeys. The application of celastrol cream to lesions showed significant improvement in the monkeys' skin erythema and scaling (Fig. 7A), epidermal thickness and inflammatory cell infiltration (Fig. 7B). Ultrasound monitoring of their skin showed that celastrol inhibited IMQ-induced epidermal thickening as well as vascularisation grading (Fig. 7C−E). Celastrol also prevented the co-localization of LRP1 and p-c-Jun (Fig. 7F). Therefore, topical celastrol cream has the potential to treat psoriasis.

4. Discussion

Although there is no cure for recurrent and untreated psoriasis, antibody-based drugs have demonstrated promising therapeutic effects for moderate to severe psoriasis patients[31]. However, about 50%−70% of psoriatic patients are mild, and antibody-based drugs are not suitable, so there is a pressing need to develop effective and safe small-molecule drugs for the treatment of psoriasis. In our study, we found that celastrol can effectively improve psoriasis-like skin inflammation in mice and, notably, celastrol cream can reduce psoriasis-like symptoms in cynomolgus monkeys when applied topically, indicating that celastrol has great potential to be developed as a topical drug for psoriasis. The production of topical preparations not only maintains celastrol's good therapeutic effects but also greatly

reduces its toxicity, and the treatment of psoriasis with celastrol cream is worth anticipating. Further optimization of the nanocarrier delivery might accelerate the clinical application of celastrol[32].

LRP1 is a cell surface protein belonging to the endocytic receptor, a member of the LDL receptor gene family[33]. It plays a crucial role in cellular lipid homeostasis, the clearance of chylomicron remnants and activated LRPAP1 (α2-macroglobulin), and the local metabolism of the plasminogen activator-plasminogen inhibitor complex[34−36]. Additionally, LRP1 regulates various cellular processes, including the metabolism of amyloid precursor protein, kinase-dependent intracellular signaling, neuronal calcium signaling, and neurotransmission[37−39]. Recent findings indicate that LRP1 is a key modulator of the Notch pathway, where its inhibition suppresses Notch signaling and reduces tumorigenesis in leukemia models[40]. Moreover, LRP1 is a crucial regulator of tau protein transport in the brain, and lowering LRP1 levels significantly inhibits the uptake and diffusion of tau protein in neurons[41]. LRP1 has been suggested as a potential therapeutic target for treating tau protein-related neurodegenerative diseases[39,41]. Contrary to previous studies, we found that LRP1 can promote fibroblast-macrophage interactions and thus exacerbate psoriasis by regulating the expression of CCL2, a key chemokine in skin fibroblasts. We also found that the targeted inhibition of LRP1 with celastrol significantly improved psoriasis-like symptoms in mice and cynomolgus monkeys, so we have high hopes for LRP1 as a target for psoriasis treatment. In addition, we also found the existence of multiple targets for celastrol, as shown in Fig. 6J, after treatment with celastrol on LRP1 knockout fibroblasts, cocultured with macrophages could further inhibit IL-23 production by macrophages.

Recent in-depth studies have yielded a more comprehensive understanding of psoriasis pathogenesis, wherein immune cells are recognized as playing a pivotal role[42−46]. Single-cell multi-omics sequencing of both psoriatic and healthy skin has uncovered the immunomodulatory function of fibroblasts. Specifically, fibroblasts within the microenvironment of psoriatic lesions are implicated in recruiting immune cells, thereby sustaining inflammation and exacerbating the progression of psoriasis. Several studies have reported that fibroblasts were involved in skin pathophysiology as local pro-inflammatory cues by regulating immune cells *via* cytokine/chemokine secretion[47]. Besides, T cells significantly increased in psoriatic lesions compared to normal skin, consistent with the pro-inflammation function of fibroblasts by promoting T cells residency and inflammation[48]. Ma et al.[49] found that a subpopulation of $SFRP2^+$ fibroblasts in psoriasis patients transitions to a pro-inflammatory state, generating CCL13. These fibroblasts interact with nearby $CCR2^+$ myeloid cells through ligand−receptor interactions, thereby amplifying the immune network. This study highlights the role of fibroblasts in psoriasis through a multi-omics analysis, and our study, in conjunction with molecular pharmacology, found that fibroblasts exacerbate psoriasis progression by recruiting macrophage interactions through the secretion of CCL2, partially corroborating the study of Ma et al. In the current study, anti-inflammatory alone did not prevent the chronic progression of psoriasis, and blocking the interactions between immune and stromal cells in this project prevented the chronic progression of psoriasis. This finding offers a novel perspective for the investigation of persistent chronic illnesses encompassing psoriasis.

5. Conclusions

In conclusion, our study elucidates the pathological mechanism through which fibroblast-macrophage interactions exacerbate psoriasis progression, and identifies LRP1 as a novel therapeutic target for psoriasis treatment.

Data availability

All data related to this study are included in the paper or the supporting information. The scRNA-seq data, spatial transcriptome data, and scATAC-seq data for human skin tissue are deposited in the GEO database under accession number GSE230842 (NCBI tracking system #23874812). Partial scRNA-seq data can be obtained in the GEO database under accession number GSE173706. The scRNA-seq data for mouse skin tissue are deposited under accession number GSE231728 (NCBI tracking system #23872713).

Acknowledgments

We acknowledge the patients and patients' families for participating in this study. We would like to thank Meijing Wang for technical assistance for MST. This work was supported by the National Key Research and Development Plan (2022YFC3500202, China), the National Natural Science Foundation of China (Nos. 82230116, 81872877, 82204715, 81803142, 82404639, and 82073975), the Natural Science Foundation of Jiangsu Province (No. BK20220476, China), the Jiangsu Provincial Double-Innovation Doctor Program (No. JSSCBS20220477, China), the Natural Science Foundation of Nanjing University of Chinese Medicine (No. XPT82204715, China), the Fundamental Research Funds for the Central Universities (Nos. 020814380179 and 020814380174, China), the Fundamental Science (Natural Science) Research Project of the Jiangsu Higher Education Institutions of China (No. 22KJB360005), the Innovation Project of Guangdong Provincial Education Department (No. 2023KTSCX320, China), the Shenzhen Science and Technology Program (Nos. 20231126130044001 and 20230731094501002, China), the School of Life Science (NJU)-Sipimo Joint Funds, and the Mountain-Climbing Talents Project of Nanjing.

Author contributions

Yuyu Zhu: Writing − original draft, Funding acquisition, Formal analysis, Data curation. Lixin Zhao: Formal analysis, Data curation. Wei Yan: Data curation. Hongyue Ma: Conceptualization. Wanjun Zhao: Formal analysis. Jiao Qu: Formal analysis. Wei Zheng: Formal analysis. Chenyang Zhang: Formal analysis. Haojie Du: Formal analysis. Meng Yu: Methodology. Ning Wan: Methodology. Hui Ye: Conceptualization. Yicheng Xie: Conceptualization. Bowen Ke: Conceptualization. Qiang Xu: Conceptualization. Haiyan Sun: Project administration, Conceptualization. Yang Sun: Writing − review & editing, Project administration, Funding acquisition. Zijun Ouyang: Writing − original draft, Project administration, Conceptualization.

Conflicts of interest

The authors declare that they have no competing interests.

Appendix A. Supporting information

Supporting information to this article can be found online at https://doi.org/10.1016/j.apsb.2024.12.041.

References

1. Boehncke WH, Schön MP. Psoriasis. *Lancet* 2015;**386**:983−94.
2. Griffiths CE, Armstrong AW, Gudjonsson JE, Barker JNWN. Psoriasis. *Lancet* 2021;**397**:1301−15.
3. Rachakonda TD, Schupp CW, Armstrong AW. Psoriasis prevalence among adults in the United States. *J Am Acad Dermatol* 2014;**70**:512−6.
4. Rendon A, Schäkel K. Psoriasis pathogenesis and treatment. *Int J Mol Sci* 2019;**20**:1475.
5. Duvallet E, Semerano L, Assier E, Falgarone G, Boissier MC. Interleukin-23: a key cytokine in inflammatory diseases. *Ann Med* 2011;**43**: 503−11.
6. Ganguly D, Haak S, Sisirak V, Reizis B. The role of dendritic cells in autoimmunity. *Nat Rev Immunol* 2013;**13**:566−77.
7. Ghoreschi K, Balato A, Enerbäck C, Sabat R. Therapeutics targeting the IL-23 and IL-17 pathway in psoriasis. *Lancet* 2021;**397**:754−66.
8. Konya V, Czarnewski P, Forkel M, Rao A, Kokkinou E, Villablanca EJ, et al. Vitamin D downregulates the IL-23 receptor pathway in human mucosal group 3 innate lymphoid cells. *J Allergy Clin Immunol* 2018;**141**:279−92.
9. Shabgah AG, Navashenaq JG, Shabgah OG, Mohammadi H, Sahebkar A. Interleukin-22 in human inflammatory diseases and viral infections. *Autoimmun Rev* 2017;**16**:1209−18.
10. Breul SD, Bradley KH, Hance AJ, Schafer MP, Berg RA, Crystal RG. Control of collagen production by human diploid lung fibroblasts. *J Biol Chem* 1980;**255**:5250−60.
11. Karsdal MA, Nielsen SH, Leeming DJ, Langholm LL, Nielsen MJ, Manon-Jensen T, et al. The good and the bad collagens of fibrosis—their role in signaling and organ function. *Adv Drug Deliv Rev* 2017;**121**:43−56.
12. Davidson S, Coles M, Thomas T, Kollias G, Ludewig B, Turley S, et al. Fibroblasts as immune regulators in infection, inflammation and cancer. *Nat Rev Immunol* 2021;**21**:704−17.
13. Wei K, Nguyen HN, Brenner MB. Fibroblast pathology in inflammatory diseases. *J Clin Invest* 2021;**131**:e149538.
14. Xu Z, Chen D, Hu Y, Jiang K, Huang H, Du Y, et al. Anatomically distinct fibroblast subsets determine skin autoimmune patterns. *Nature* 2022;**601**:118−24.
15. Łuczaj W, Wroński A, Domingues P, Domingues MR, Skrzydlewska E. Lipidomic analysis reveals specific differences between fibroblast and keratinocyte ceramide profile of patients with psoriasis vulgaris. *Molecules* 2020;**25**:E630.
16. He X, Shen C, Lu Q, Li J, Wei Y, He L, et al. Prokineticin 2 plays a pivotal role in psoriasis. *EBioMedicine* 2016;**13**:248−61.
17. Nedoszytko B, Sokołowska-Wojdyło M, Ruckemann-Dziurdzińska K, Roszkiewicz J, Nowicki RJ. Chemokines and cytokines network in the pathogenesis of the inflammatory skin diseases: atopic dermatitis, psoriasis and skin mastocytosis. *Postepy Dermatol Alergol* 2014;**31**: 84−91.
18. Kim J, Lee J, Kim HJ, Kameyama N, Nazarian R, Der E, et al. Single-cell transcriptomics applied to emigrating cells from psoriasis elucidate pathogenic *versus* regulatory immune cell subsets. *J Allergy Clin Immunol* 2021;**148**:1281−92.
19. Lou F, Sun Y, Xu Z, Niu L, Wang Z, Deng S, et al. Excessive polyamine generation in keratinocytes promotes Self-RNA sensing by dendritic cells in psoriasis. *Immunity* 2020;**53**:204−16.e10.
20. Rizzo HL, Kagami S, Phillips KG, Kurtz SE, Jacques SL, Blauvelt A. IL-23-mediated psoriasis-like epidermal hyperplasia is dependent on IL-17A. *J Immunol* 2011;**186**:1495−502.
21. Zhu Y, Wan N, Shan X, Deng G, Xu Q, Ye H, et al. Celastrol targets adenylyl cyclase-associated protein 1 to reduce macrophages-mediated inflammation and ameliorates high fat diet-induced metabolic syndrome in mice. *Acta Pharm Sin B* 2021;**11**:1200−12.
22. Martinez Molina D, Jafari R, Ignatushchenko M, Seki T, Larsson EA, Dan C, et al. Monitoring drug target engagement in cells and tissues using the cellular thermal shift assay. *Science* 2013; **341**:84−7.
23. Vestergaard C, Just H, Baumgartner Nielsen J, Thestrup-Pedersen K, Deleuran M. Expression of CCR2 on monocytes and macrophages in chronically inflamed skin in atopic dermatitis and psoriasis. *Acta Derm Venereol* 2004;**84**:353−8.
24. Yang H, Zhang Q, Xu M, Wang L, Chen X, Feng Y, et al. CCL2−CCR2 axis recruits tumor associated macrophages to induce immune evasion through PD-1 signaling in esophageal carcinogenesis. *Mol Cancer* 2020;**19**:41.
25. Georgakis MK, Bernhagen J, Heitman LH, Weber C, Dichgans M. Targeting the CCL2−CCR2 axis for atheroprotection. *Eur Heart J* 2022;**43**:1799−808.
26. Lillis AP, Van Duyn LB, Murphy-Ullrich JE, Strickland DK. LDL receptor-related protein 1: unique tissue-specific functions revealed by selective gene knockout studies. *Physiol Rev* 2008;**88**:887−918.
27. Bang YJ, Hu Z, Li Y, Gattu S, Ruhn KA, Raj P, et al. Serum amyloid A delivers retinol to intestinal myeloid cells to promote adaptive immunity. *Science* 2021;**373**:eabf9232.
28. Novoszel P, Holcmann M, Stulnig G, De Sa Fernandes C, Zyulina V, Borek I, et al. Psoriatic skin inflammation is promoted by c-Jun/AP-1-dependent CCL2 and IL-23 expression in dendritic cells. *EMBO Mol Med* 2021;**13**:e12409.
29. Wolter S, Doerrie A, Weber A, Schneider H, Hoffmann E, von der Ohe J, et al. c-Jun controls histone modifications, NF-kappaB recruitment, and RNA polymerase II function to activate the *CCL2* gene. *Mol Cell Biol* 2008;**28**:4407−23.
30. Zhu Y, Wu Z, Yan W, Shao F, Ke B, Jiang X, et al. Allosteric inhibition of SHP2 uncovers aberrant TLR7 trafficking in aggravating psoriasis. *EMBO Mol Med* 2022;**14**:e14455.
31. Norden A, Moon JY, Javadi SS, Munawar L, Maul JT, Wu JJ. Anti-drug antibodies of IL-23 inhibitors for psoriasis: a systematic review. *J Eur Acad Dermatol Venereol* 2022;**36**:1171−7.
32. Chan CL, Sun Y, Mao X, Chen H, Zhao J, Rong J. Druggability, molecular targets, and nanocarrier delivery of natural triterpenoid celastrol against chronic diseases. *Acta Materia Med* 2024;**3**: 383−404.
33. Herz J, Hamann U, Rogne S, Myklebost O, Gausepohl H, Stanley KK. Surface location and high affinity for calcium of a 500-kd liver membrane protein closely related to the LDL-receptor suggest a physiological role as lipoprotein receptor. *EMBO J* 1988; **7**:4119−27.
34. Etique N, Verzeaux L, Dedieu S, Emonard H. LRP-1: a checkpoint for the extracellular matrix proteolysis. *BioMed Res Int* 2013;**2013**:152163.
35. Lillis AP, Mikhailenko I, Strickland DK. Beyond endocytosis: LRP function in cell migration, proliferation and vascular permeability. *J Thromb Haemost* 2005;**3**:1884−93.
36. Aldahmesh MA, Khan AO, Alkuraya H, Adly N, Anazi S, Al-Saleh AA, et al. Mutations in LRPAP1 are associated with severe myopia in humans. *Am J Hum Genet* 2013;**93**:313−20.
37. Pencheva N, Tran H, Buss C, Huh D, Drobnjak M, Busam K, et al. Convergent multi-miRNA targeting of ApoE drives LRP1/LRP8-dependent melanoma metastasis and angiogenesis. *Cell* 2012;**151**: 1068−82.
38. Misu H, Takayama H, Saito Y, Mita Y, Kikuchi A, Ishii K-A, et al. Deficiency of the hepatokine selenoprotein P increases responsiveness to exercise in mice through upregulation of reactive oxygen species and AMP-activated protein kinase in muscle. *Nat Med* 2017;**23**:508−16.
39. Tachibana M, Holm ML, Liu CC, Shinohara M, Aikawa T, Oue H, et al. APOE4-mediated amyloid-β pathology depends on its neuronal receptor LRP1. *J Clin Invest* 2019;**129**:1272−7.
40. Bian W, Tang M, Jiang H, Xu W, Hao W, Sui Y, et al. Low-density-lipoprotein-receptor-related protein 1 mediates Notch pathway activation. *Dev Cell* 2021;**56**:2902−19.e8.

41. Rauch JN, Luna G, Guzman E, Audouard M, Challis C, Sibih YE, et al. LRP1 is a master regulator of tau uptake and spread. *Nature* 2020;**580**:381−5.
42. Liu Y, Wang H, Taylor M, Cook C, Martínez-Berdeja A, North JP, et al. Classification of human chronic inflammatory skin disease based on single-cell immune profiling. *Sci Immunol* 2022;**7**:eabl9165.
43. Zhang B, Roesner LM, Traidl S, Koeken VACM, Xu CJ, Werfel T, et al. Single-cell profiles reveal distinctive immune response in atopic dermatitis in contrast to psoriasis. *Allergy* 2023;**78**:439−53.
44. Sato Y, Ogawa E, Okuyama R. Role of innate immune cells in psoriasis. *Int J Mol Sci* 2020;**21**:6604.
45. Wu R, Zeng J, Yuan J, Deng X, Huang Y, Chen L, et al. MicroRNA-210 overexpression promotes psoriasis-like inflammation by inducing Th1 and Th17 cell differentiation. *J Clin Invest* 2018;**128**:2551−68.
46. Yin L, Zhang E, Mao T, Zhu Y, Ni S, Li Y, et al. Macrophage P2Y6R activation aggravates psoriatic inflammation through IL-27-mediated Th1 responses. *Acta Pharm Sin B* 2024;**14**:4360−77.
47. Cai X, Han M, Lou F, Sun Y, Yin Q, Sun L, et al. Tenascin C^+ papillary fibroblasts facilitate neuro-immune interaction in a mouse model of psoriasis. *Nat Commun* 2023;**14**:2004.
48. Dong C, Lin J-M, Lu X, Zhu J, Lin L, Xu J, et al. Fibroblasts with high matrix metalloproteinase 2 expression regulate $CD8^+$ T-cell residency and inflammation *via* CD100 in psoriasis. *Br J Dermatol* 2024;**191**:405−18.
49. Ma F, Plazyo O, Billi AC, Tsoi LC, Xing X, Wasikowski R, et al. Single cell and spatial sequencing define processes by which keratinocytes and fibroblasts amplify inflammatory responses in psoriasis. *Nat Commun* 2023;**14**:3455.